CMS Physics Analysis Summary

Contact: cms-pag-conveners-susy@cern.ch 2012/07/14

Search for supersymmetery in final states with missing transverse energy and 0, 1, 2, or $\geq$ 3 b jets in 7 TeV pp collisions

The CMS Collaboration

Abstract

A search for supersymmetry in the jets and missing transverse energy final state is performed in pp collisions at a centre of mass energy of $\sqrt{s} = 7$ TeV. The data sample corresponds to an integrated luminosity of 4.98 fb^{-1} collected by the CMS experiment at the LHC. In this search, a kinematic variable, α_{T}, is used as the main discriminator between events with genuine and misreconstructed missing transverse energy. The search is performed in a signal region that is binned in the scalar sum of the transverse energy of jets and the number of jets identified as originating from a bottom quark. No excess of events over the standard model expectation is found. Exclusion limits are set in the parameter space of the constrained minimal supersymmetric extension of the standard model, and also in simplified models, with a special emphasis on third generation and compressed spectra scenarios.

1 Introduction

Supersymmetry (SUSY) is generally regarded as one of the most likely extensions to the Standard Model of particle physics (SM) [1–8]. It is a well-establised theory based on the unique extension of the space-time symmetry group underpinning the SM, introducing a relationship between fermions and bosons.

A low-energy realisation of SUSY, e.g. at the TeV scale, is motivated by the cancellation of the quadratically divergent loop corrections to the Higgs boson mass in the SM [7, 8]. These corrections are proportional to the masses of the particles that couple to the Higgs boson. The most relevant terms come from the interplay between the masses of the third generation (top and bottom) squarks, and the largest Yukawa coupling (of the top quark).

In order to avoid large cancellations in these loop corrections, the mass difference between the top quark and the third generation squarks must not be too large [9]. Therefore, whilst the majority of SUSY particles might not be accessible at the LHC, the existence of a low mass Higgs boson would motivate top and bottom squark production, with subsequent decays to their SM partners, to take place at the TeV scale.

Furthermore, if the multiplicative quantum number R-parity is conserved [10], SUSY particles such as squarks and gluinos are produced in pairs and decay to the lightest SUSY particle (LSP), which is generally assumed to be a weakly interacting massive particle. This results in a final state signature that is rich in jets, especially those originating from bottom quarks, and also contains a significant amount of missing transverse energy.

This document summarises a search which is designed to be sensitive to missing transverse energy signatures in events with two or more energetic jets that are categorised according to the number of reconstructed jets originating from bottom quarks (b jets) per event. With respect to previous searches following the same general inclusive search strategy [11, 12], this refinement provides improved sensitivity to third generation squark signatures. It also maintains the ability to identify a wide variety of SUSY event topologies, which arise from the main production mechanisms of massive coloured sparticles at the LHC, namely squark-squark, squark-gluino and gluino-gluino interactions.

In 2010 and 2011 the CMS and ATLAS experiments performed various searches [11–19] for the production of massive coloured sparticles and their subsequent decay to a final state of jets and missing transverse energy. These searches were performed with a dataset of pp collisions at $\sqrt{s} = 7$ TeV, and no significant deviations from SM expectations were observed. The majority of these searches have been interpreted in the context of a specific model of SUSY-breaking, the constrained minimal supersymmetric extension of the standard model (CMSSM) [20–22]. The CMSSM is described by the following five parameters: the universal scalar and gaugino mass parameters, m_0 and $m_{1/2}$; the universal trilinear soft SUSY-breaking parameter, A_0; the ratio of the vacuum expectation values of the two Higgs doublets, $\tan\beta$; and the sign of the Higgs mixing parameter, μ. The simplifying assumption of universality at an energy scale of $\mathcal{O}(10^{16})$ GeV makes the CMSSM a useful framework to study SUSY phenomenology at colliders, and to benchmark the performance of experimental searches.

On the other hand, the universality conditions of the CMSSM result in significant restrictions on the possible SUSY particle mass spectra, leading to a limitation on the possible kinematic signatures arising in the context of the CMSSM. This limits the interpretation of results in certain scenarios, particularly compressed spectra, where the mass difference between the primary produced sparticle (e.g. a squark or a gluino) and the LSP is rather small, and in the context of third generation squarks. Therefore, in order to complement the interpretation within the

CMSSM, simplified models [23–25] are also used to interpret the search results presented below. These models are characterised using a limited set of SUSY particles (production and decay) and enable comprehensive studies of individual SUSY event topologies. These studies can be performed without limitations on fundamental kinematic properties such as decay modes, production cross sections, and sparticle masses. Below, a special emphasis in the interpretation is placed on constraints arising on both third generation squark production and compressed SUSY spectra.

2 The CMS apparatus

The central feature of the CMS detector is a superconducting solenoid, which provides an axial magnetic field of 3.8 T. The bore of the solenoid is instrumented with several particle detection systems. Silicon pixel and strip tracking systems measure charged particle trajectories with full azimuthal (ϕ) coverage and a pseudorapidity acceptance of $|\eta| < 2.5$, where $\eta \equiv -\ln[\tan(\theta/2)]$ and θ is the polar angle with respect to the counterclockwise beam direction. The resolutions on the transverse momentum and impact parameter of a charged particle with $p_{\mathrm{T}} < 40\,\mathrm{GeV}$ are typically 1% and 15 μm, respectively. A lead tungstate crystal electromagnetic calorimeter (ECAL) and a brass/scintillator hadron calorimeter surround the tracking volume. The forward region is covered by an iron/quartz-fiber hadron calorimeter. The ECAL covers $|\eta| < 3.0$ and provides an energy resolution of better than 0.5% for unconverted photons with transverse energies above 100 GeV. The hadron calorimeters cover $|\eta| < 5.0$ with a resolution in jet energy, E (GeV), of about $100\%/\sqrt{\mathrm{E}}$. Muons are identified in gas-ionization detectors, covering $|\eta| < 2.4$, embedded in the steel return yoke. The CMS detector is nearly hermetic, which allows for momentum-balance measurements in the plane transverse to the beam axis. A two-tier trigger system is designed to select the most interesting pp collision events for use in physics analysis. A detailed description of the CMS detector can be found elsewhere [26].

3 Object definition

The offline selection criteria and event reconstruction follows the procedure described in [11, 12]. Jets are reconstructed from energy deposits in the calorimeter towers, clustered by the anti-k_{T} algorithm [27] with a size parameter of 0.5. The raw jet energies measured by the calorimeter systems are corrected to establish a uniform relative response in η and a calibrated absolute response in transverse momentum p_{T} with an associated uncertainty between 2% and 4%, depending on the jet η and p_{T} [28]. Jets considered in the analysis are required to have transverse energy $E_{\mathrm{T}} > 50\,\mathrm{GeV}$. The highest-$E_{\mathrm{T}}$ jet is additionally required to be within the central tracker acceptance ($|\eta| < 2.5$) and the two highest-E_{T} jets must also each have $E_{\mathrm{T}} > 100\,\mathrm{GeV}$. Events are vetoed if any additional jet satisfies both $E_{\mathrm{T}} > 50\,\mathrm{GeV}$ and $|\eta| > 3$, or rare, spurious signals are identified in the calorimeters [29, 30]. To suppress SM processes with genuine $\not\!\!E_{\mathrm{T}}$ from neutrinos, events containing an isolated electron [31] or muon [32] with $p_{\mathrm{T}} > 10\,\mathrm{GeV}$ are vetoed. To select a pure multi-jet topology, events are vetoed in which an isolated photon [33] with $p_{\mathrm{T}} > 25\,\mathrm{GeV}$ is found.

The presence of a b jet is identified through a vertex that is displaced with respect to the primary interaction, using an algorithm that attempts to reconstruct a secondary vertex from charged particles associated to each jet. Using a likelihood ratio technique, the combined secondary vertex algorithm [34] incorporates several variables related to the vertex, such as decay length significance, mass, and track multiplicity, to build a discriminator between jets originating from bottom quarks and other sources. These include jets from c quarks and light-flavour quarks.

The algorithm also provides a value for this discriminator based on single track properties, when no secondary vertices have been reconstructed. Discriminator values above a certain threshold are used to tag jets as reconstructed b jets. This threshold is chosen such that the mis-tagging rate, i.e. the probability to tag jets originating from light-flavour quarks as b jets, is approximately 1% for jets with transverse momenta of 100 GeV [34, 35]. This typically results in a b tagging efficiency, i.e. the probability to correctly tag jets originating from b quarks, in the range $60 - 70\%$ [34, 35].

The following two variables characterize the visible energy and missing momentum in the transverse plane: the scalar sum of the transverse energy E_{T} of jets, defined as $H_{\mathrm{T}} = \sum_{i=1}^{N_{\mathrm{jet}}} E_{\mathrm{T}}$, and the magnitude of the vector sum of the transverse momenta $\vec{p_{\mathrm{T}}}$ of jets, defined as $\not{H}_{\mathrm{T}} = |\sum_{i=1}^{N_{\mathrm{jet}}} \vec{p_{\mathrm{T}}}|$, where N_{jet} is the number of jets with $E_{\mathrm{T}} > 50\,\mathrm{GeV}$. Significant hadronic activity in the event is ensured by requiring $H_{\mathrm{T}} > 275\,\mathrm{GeV}$. Following these selections, the background from multi-jet production, a manifestation of quantum chromodynamics (QCD), is still several orders of magnitude larger than the typical signal expected from SUSY.

4 Selection of multi-jet events with missing transverse energy

The α_{T} kinematic variable, first introduced in Refs. [36–38], is used in the selection of multi-jet events to efficiently reject events either without significant $\not{E}_{\mathrm{T}}$ or with transverse energy mis-measurements, whilst retaining a large sensitivity to new physics with genuine $\not{E}_{\mathrm{T}}$ signatures. For dijet events, the α_{T} variable is defined as:

$$\alpha_{\mathrm{T}} = \frac{{E_{\mathrm{T}}}^{\mathrm{j}2}}{M_{\mathrm{T}}} \quad , \quad M_{\mathrm{T}} = \sqrt{\left(\sum_{i=1}^{2} {E_{\mathrm{T}}}^{\mathrm{j}i}\right)^2 - \left(\sum_{i=1}^{2} p_x^{\mathrm{j}i}\right)^2 - \left(\sum_{i=1}^{2} p_y^{\mathrm{j}i}\right)^2}. \tag{1}$$

where ${E_{\mathrm{T}}}^{\mathrm{j}2}$ is the transverse energy of the least energetic jet of the two, and M_{T} is the transverse mass of the dijet system. For a perfectly measured dijet event with ${E_{\mathrm{T}}}^{\mathrm{j}1} = {E_{\mathrm{T}}}^{\mathrm{j}2}$ and jets back-to-back in ϕ, and in the limit in which each jet's momentum is large compared with its mass, the value of α_{T} is 0.5. In the case of an imbalance in the measured transverse energies of back-to-back jets, α_{T} is smaller than 0.5. Values significantly greater than 0.5 are observed when the two jets are not back-to-back, recoiling against genuine $\not{E}_{\mathrm{T}}$.

For events with three or more jets, an equivalent dijet system is formed by combining the jets in the event into two pseudo-jets. The E_{T} of each of the two pseudo-jets is calculated as the scalar sum of the measured E_{T} of the contributing jets. The combination chosen is the one that minimizes the E_{T} difference (ΔH_{T}) between the two pseudo-jets. This simple clustering criterion provides the best separation between multi-jet events and events with genuine $\not{E}_{\mathrm{T}}$. Thus, in the case of events with at least three jets, the α_{T} variable can be defined as:

$$\alpha_{\mathrm{T}} = \frac{1}{2} \cdot \frac{H_{\mathrm{T}} - \Delta H_{\mathrm{T}}}{\sqrt{{H_{\mathrm{T}}}^2 - \not{H}_{\mathrm{T}}{}^2}} = \frac{1}{2} \cdot \frac{1 - (\Delta H_{\mathrm{T}}/H_{\mathrm{T}})}{\sqrt{1 - (\not{H}_{\mathrm{T}}/H_{\mathrm{T}})^2}} \tag{2}$$

Events with extremely rare but large stochastic fluctuations in the calorimetric measurements of jet energies can lead to values of α_{T} slightly above 0.5. Such events are rejected by requiring $\alpha_{\mathrm{T}} > 0.55$. A similar behaviour is observed in events with reconstruction failures, severe energy losses due to detector inefficiencies, or jets below the E_{T} threshold that result in significant $\not{H}_{\mathrm{T}}$ relative to the value of $\not{E}_{\mathrm{T}}$ (as measured by the calorimeter systems, which is not affected by

jet E_T thresholds). These classes of events are rejected by applying dedicated vetoes, described further in Ref. [12]. The leakage above 0.5 becomes smaller with increasing H_T. This is due in part to increasing average jet energy and thus improving jet energy resolution. Further, the relative impact of jets falling below the E_T threshold is reduced as the scale of the event (i.e. H_T) increases.

The signal region is defined by $H_T > 275\,\text{GeV}$ and $\alpha_T > 0.55$, which is divided into eight bins in H_T: two bins of width 50 GeV in the range $275 < H_T < 375\,\text{GeV}$, five bins of width 100 GeV in the range $375 < H_T < 875\,\text{GeV}$, and a final open bin, $H_T > 875\,\text{GeV}$. As in Ref. [12], the jet E_T threshold is scaled down to 37 GeV and 43 GeV for the regions $275 < H_T < 325\,\text{GeV}$ and $325 < H_T < 375\,\text{GeV}$, respectively. The highest-E_T jet threshold is also scaled accordingly. This is done in order to maintain a background composition and event kinematics similar to those observed for the higher H_T bins. Events are further categorised according to whether they contain exactly zero, one, two, or at least three reconstructed b jets.

Events in the signal sample are recorded with a dedicated trigger condition that must satisfy simultaneously the requirements $H_T > 250\,\text{GeV}$ and $\alpha_T > 0.53$, with the latter threshold increasing with time to 0.60 due to higher instantaneous luminosities observed towards the end of 2011. The efficiency with which events that satisfy the signal sample selection criteria also satisfy the trigger conditions is measured to be $82.8 \pm 1.1\,\%$, $95.9 \pm 0.9\,\%$, and $> 98.5 \pm 0.9\,\%$ for the regions $275 < H_T < 375\,\text{GeV}$, $325 < H_T < 375\,\text{GeV}$, and $H_T > 375\,\text{GeV}$, respectively.

A disjoint hadronic control sample consisting predominantly of multi-jet events is defined by inverting the α_T requirement for a given H_T region, which is used primarily in the estimation of any residual background from multi-jet events. These events are recorded by a set of triggers with thresholds in H_T.

5 Background estimation from data

Once all selection requirements have been imposed, the contribution from multi-jet events is expected to be negligible. The remaining significant backgrounds in the hadronic signal region stem from SM processes with genuine $\not{E}_T$ in the final state. In the case of events where no b jets are identified, the largest backgrounds with genuine $\not{E}_T$ arise from the production of W and Z bosons in association with jets. The weak decay $Z \to \nu\bar{\nu}$ is the only relevant contribution from Z+jets events. For W+jets events, the two relevant sources are leptonic W decays in which the lepton is not reconstructed or fails the isolation or acceptance requirements, and the weak decay $W \to \tau\nu$ where the τ decays hadronically and is identified as a jet. For events with one or more reconstructed b jets however, top quark production followed by semi-leptonic weak decays becomes the most important single background source. For events with only one reconstructed b jet, the contribution of both W + jets and Z + jets backgrounds are of a similar size to the top background. For events with two reconstructed b jets, $t\bar{t}$ production dominates, whilst events with three or more reconstructed b jets originate almost exclusively from $t\bar{t}$ events, in which one or several jets are misidentified as b jets.

In order to estimate the contributions from each of these backgrounds, three data control samples are used, which are binned in the same way as the signal sample. A μ + jets data sample provides an estimate of the contributions from $t\bar{t}$ and W production, leading to W + jets final states, and other small contributions from SM backgrounds such as single top, di-boson, and $Z\to$ $\mu\mu$ + jets production. The remaining irreducible background of $Z \to \nu\bar{\nu}$ + jets events in the hadronic signal region is estimated from both a data sample of $Z \to \mu\mu$ + jets and γ + jets events, which share kinematic properties but have different acceptances. The $Z \to \mu\mu$ +

jets events have identical kinematic properties when the two muons are ignored, but a smaller branching ratio, while the γ + jets events have similar kinematic properties when the photon is ignored [39, 40], but a larger production cross section. The event selection criteria for the control samples are defined to ensure that any potential contamination from multi-jet events is negligible. Further, the selection also suppress signal contamination from a wide variety of SUSY models, including those considered in this analysis, to a negligible level.

5.1 Definition of data control samples

The μ + jets sample is recorded using two different trigger strategies, to account for evolving trigger conditions during the 2011 run. The hadronic trigger condition, combining H_T and α_T, is used for the region $H_T < 375\,\text{GeV}$. Here, the event selection, following closely the prescription described in Ref. [41], requires exactly one isolated muon that satisfies stringent quality criteria, with $p_T > 10\,\text{GeV}$ and $|\eta| < 2.1$. In order for the trigger to be maximally efficient, the requirement $\alpha_T > 0.55$ is imposed.

For the region $H_T > 375\,\text{GeV}$, the trigger condition requires both a muon above a p_T threshold as high as 40 GeV and $H_T > 300\,\text{GeV}$. The muon must satisfy $p_T > 45\,\text{GeV}$ in order for the trigger efficiency to be high at $91.3 \pm 0.1\,\%$. The requirement $\alpha_T > 0.55$ is imposed when zero b jets are reconstructed per event; for all other event categories, in which at least one b jet is reconstructed, no α_T requirement is used in order to increase yields in the presence of b jets.

Further selection criteria are applied. The transverse mass of the muon and $\not\!\!E_T$ system must be larger than 30 GeV to ensure a sample rich in W bosons. The muon is required to be separated from the closest jet in the event by $\Delta\eta$ and $\Delta\phi$ such that the distance $\Delta R \equiv \sqrt{\Delta\eta^2 + \Delta\phi^2} > 0.5$. To ensure that this sample is disjoint from the $\mu\mu$ + jets sample, the event is rejected if a second muon candidate is identified that does not satisfy all quality criteria or is non-isolated or is outside acceptance, and the two muon candidates have an invariant mass that is within a window of $\pm 25\,\text{GeV}$ around the mass of the Z boson.

The $\mu\mu$ + jets sample follows the same trigger strategy and muon identification criteria as the μ + jets sample. The event selection requires exactly two oppositely charged, isolated muons satisfying stringent quality criteria, and an invariant mass within a window of $\pm 25\,\text{GeV}$ around the mass of the Z boson. Each muon is required to be separated from the nearest jet in the event by the distance $\Delta R > 0.5$. The same α_T requirements are used as for the μ + jets sample.

The γ + jets sample is selected using a dedicated photon trigger condition requiring a localized, large energy deposit in the ECAL with $E_T > 135\,\text{GeV}$ that satisfies loose photon identification and isolation criteria [33]. The offline selection requires $H_T > 375\,\text{GeV}$, $\alpha_T > 0.55$, and a single photon to be reconstructed with $E_T > 150\,\text{GeV}$, $|\eta| < 1.45$, satisfying tight isolation criteria, and with a minimum distance to any jet of $\Delta R > 1.0$. For these selection criteria, the photon trigger condition is found to be fully efficient.

5.2 Method for estimating genuine $\not\!\!E_T$ background

The method used to estimate the SM background contributions in the hadronic signal region relies on the use of translation factors, which are constructed per data control sample per bin in the two dimensions of H_T and number of reconstructed b jets per event, n_b^{reco}. These translation factors are determined from simulation samples generated with PYTHIA 6 [42], MADGRAPH v4.22 [43], and the GEANT-based [44] CMS detector simulation. Each factor is defined as the ratio of yields from simulation in a given bin of the hadronic signal sample ($N_{\text{MC}}^{\text{signal}}$) and the corresponding bin of one control sample ($N_{\text{MC}}^{\text{control}}$). The factors are used to translate the ob-

served yield measured in a control sample bin ($N_{\text{obs}}^{\text{control}}$) into an expectation for one or more SM background processes in the corresponding bin of the hadronic signal sample ($N_{\text{pred}}^{\text{signal}}$):

$$N_{\text{pred}}^{\text{signal}}(H_{\text{T}}, n_{\text{b}}^{\text{reco}}) = N_{\text{obs}}^{\text{control}}(H_{\text{T}}, n_{\text{b}}^{\text{reco}}) \times \frac{N_{\text{MC}}^{\text{signal}}}{N_{\text{MC}}^{\text{control}}}(H_{\text{T}}, n_{\text{b}}^{\text{reco}}). \tag{3}$$

The $\mu\mu$ + jets and γ + jets control samples are used to predict only the background contribution from the $Z \to \nu\bar{\nu}$ + jets process. The μ + jets sample is used to predict the background contributions from W + jets and $t\bar{t}$, as well as small contributions from all other relevant SM processes, which include single top, di-boson, and $Z \to \mu\mu$ + jets production.

The number of reconstructed b jets per event ($n_{\text{b}}^{\text{reco}}$) is estimated from a method based on truth-level information contained in the simulation, namely: the numbers of jets originating from underlying b quarks, n_{b}, and from light quarks, n_{q}, per event. All relevant combinations of n_{b} and n_{q} are considered, and event counts are recorded in bins of H_{T} for each combination, $N(n_{\text{b}}, n_{\text{q}})$. The b tagging efficiency, ϵ, and a flavour-averaged mistagging rate, m, are measured also from simulation for each H_{T} bin, with both quantities averaged over jet p_{T} and η. Corrections are applied to both ϵ and m in order to match the corresponding measurements with data [34, 35]. The aforementioned information is sufficient to determine an accurate prediction for $n_{\text{b}}^{\text{reco}}$. For example, an estimate for the number of events with zero reconstructed b jets is given by the expression:

$$n_0^{\text{reco}} = \sum_{n_{\text{b}} \geq 0,\, n_{\text{q}} \geq 0} N(n_{\text{b}}, n_{\text{q}}) \times (1-\epsilon)^{n_{\text{b}}} \times (1-m)^{n_{\text{q}}} \tag{4}$$

A similar treatment is used for the other b jet multiplicity categories. The yields from simulation, binned according to H_{T} and $n_{\text{b}}^{\text{reco}}$ as determined with the method described above, are found to be in good agreement with the yields obtained directly from the simulation. The method exploits the ability to make precise measurements of $N(n_{\text{b}}, n_{\text{q}})$, ϵ and particularly m, which means that predicted event yields for a given b jet category can be made with a higher statistical precision than obtained directly from simulation. This is particularly important for events with $n_{\text{b}}^{\text{reco}} \geq 3$, which requires the presence of mistagged jets in the event. In this case, the most probable (albeit small) background is $t\bar{t}$, with two correctly tagged b jets and an additional mistagged jet.

Any mismodelling in the simulation of the event kinematics or instrumental effects observed in data are expected to largely cancel in the ratio of yields used to construct the translation factors, given that the data control and signal samples, and the corresponding event samples from simulation, are defined to be kinematically similar. However, a systematic uncertainty is assigned to each translation factor to account for theoretical uncertainties [40] and residual biases in the simulation modelling [11]. The magnitudes of the systematic uncertainties are determined from a representative set of closure tests in data, in which yields from one of the three independent control samples, along with the corresponding translation factors obtained from simulation, are used to predict the yields in another control sample, following the same prescription defined in Equation 3. The contamination from multi-jet events and any potential signal is expected to be negligible. Therefore, the closure tests carried out between control samples probe the properties of the relevant SM backgrounds.

A set of five closure tests, which probe key ingredients of the simulation modelling that may introduce biases to the translation factors, and the H_{T}-dependent systematic uncertainties are

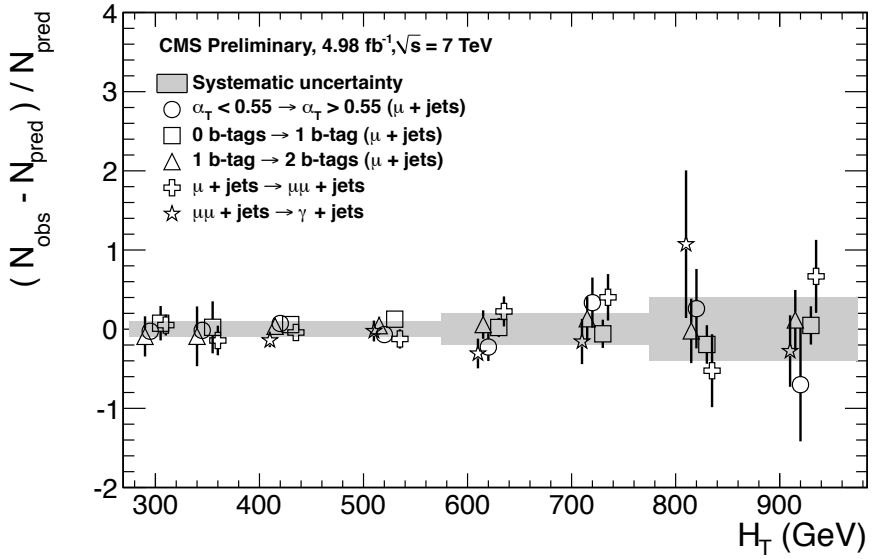

Figure 1: A set of closure tests overlaid on top of grey bands that represent the systematic uncertainties used for the three H_{T} regions in the final simultaneous fit. To account for evolving conditions throughout the data-taking period a differing trigger for μ+jets and $\mu\mu$+jets control samples is used in the first two H_{T} bins, while the trigger for the γ+jets sample is only efficient for the last six H_{T} bins.

shown in Fig. 1. The first three closure tests are carried out within the μ + jets sample, and probe the modelling of the α_{T} distribution in genuine $\not\!\!E_{\mathrm{T}}$ events (circles), the relative composition between W + jets and top events (squares), and the modelling of the reconstruction of b jets (triangles), respectively. The fourth test (crosses), connecting the μ + jets and $\mu\mu$ + jets control samples, addresses the modelling of the relative contributions of Z + jets to W + jets and top events while the fifth test (stars) deals with the consistency between the Z$\rightarrow$ $\mu\mu$ + jets and γ + jets samples.

All individual closure tests demonstrate, within the statistical precision of each test, that there are no significant biases inherent in the translation factors obtained from simulation. The level of closure achieved in these tests is used to estimate the systematic uncertainties that are assigned to the translation factors, which are determined to be 10%, 20% and 40% for the three regions $275 < H_{\mathrm{T}} < 575\,\mathrm{GeV}$, $575 < H_{\mathrm{T}} < 775\,\mathrm{GeV}$ and $H_{\mathrm{T}} > 775\,\mathrm{GeV}$, respectively.

A further dedicated study to account for potential systematic effects arising from the modelling of the reconstruction of b jets in simulation was also carried out. After correcting the efficiency and mis-tagging rates of b jets in simulation for residual differences as measured in data, the corresponding uncertainties on these corrections are propagated to the translation factors and found to be negligible. In addition, several robustness tests were performed, including treating c jets as b jets in the yield estimates throughout, as well as ignoring the contribution from hadronic tau decays. These tests also yielded negligible effects on the translation factors, highlighting their insensitivity to potential mismodellings in simulation. Therefore, the H_{T}-dependent systematic uncertainties of 10%, 20% and 40% are used for all b jet multiplicities.

6 Results

A binned likelihood fit using all four data samples is carried out to obtain a consistent prediction of the SM background. The fit maximizes the total likelihood:

$$L_{\text{total}} = L_{\text{hadronic}} \times L_{\mu+\text{jets}} \times L_{\mu\mu+\text{jets}} \times L_{\gamma+\text{jets}} \quad n_b < 3 \tag{5}$$

$$L_{\text{total}} = L_{\text{hadronic}} \times L_{\mu+\text{jets}} \quad n_b \geq 3 \tag{6}$$

simultaneously in eight bins of H_{T} and four bins of b jet multiplicity. L_{hadronic} describes the yields in the hadronic sample, while the terms $L_{\mu+\text{jets}}$, $L_{\mu\mu+\text{jets}}$, and $L_{\gamma+\text{jets}}$ describe the H_{T} and b jet multiplicity dependent yields in the μ + jets , $\mu\mu$ + jets, and γ + jets samples respectively. For each bin, the expected yields in the control samples are related to the components of the SM expectations in the hadronic signal sample via translation factors from simulation. Since for $n_b \geq 3$ the only relevant SM background arises from top events, only the μ+jets control sample is used in the likelihood to determine the background in the hadronic signal region for this b jet multiplicity. In addition, any potential contribution from multi-jet background in the hadronic sample is included using $R_{\alpha_{\text{T}}}$, which is defined as the ratio of events which result in a value of α_{T} above and below some threshold value for a given H_{T} bin. This ratio is modelled as a falling exponential function versus H_{T}, $A_{n_b} \text{e}^{-k\,H_{\text{T}}}$ [12]. Values of A_{n_b} are determined by the fit independently for each category of the number of reconstructed b jets per event. A common parameter k is used for all four b jet categories, which is constrained via measurements in a multi-jet−enriched data side-band satisfying the criteria $H_{\text{T}} < 575\,\text{GeV}$ and $0.52 < \alpha_{\text{T}} < 0.55$. The parameter k is measured to be [-2.89 ± 0.61 (stat.) ± 0.46 (syst.)] $\times 10^{-2}$. A further side band, defined by inverting the $\not{H}_{\text{T}}/\not{E}_{\text{T}}$ cleaning cut [12], is used to confirm that this method provides an unbiased estimator for k and to estimate a systematic uncertainty.

In order to test the compatibility of the observed yields with the expectations from SM processes only, the likelihood function is maximized over all parameters. The hadronic signal region yields measured in data, as well as the SM predictions obtained from the simultaneous fit across all bins of each control sample are shown in Table 1. A comparison of the observed yields and the SM expectations in bins of H_{T} for events with exactly zero, one, two, and at least three reconstructed b jets are shown in Figures 2, 3, 4 and 5, respectively, for the hadronic signal region, and the three control samples. For all four b jet categories, no significant excess above the SM expectation is observed in the hadronic signal region, and the control samples are well described by the SM hypothesis. Furthermore, all four normalization parameters A_{n_b}, used to characterise the potential multi-jet background, are found to be compatible with zero within uncertainties, confirming the hypothesis that such contributions are negligible.

Table 1: Comparison of the measured yields in the different H_T and b jet multiplicity bins for the hadronic sample with the SM expectations and combined statistical and systematic uncertainties given by the simultaneous fit.

H_T (GeV)	275–325	325–375	375–475	475–575	575–675	675–775	775–875	875–∞
0 b jets SM	2933^{+56}_{-52}	1139^{+17}_{-40}	783^{+17}_{-27}	261^{+14}_{-8}	$81.5^{+6.5}_{-6.5}$	$34.2^{+4.0}_{-3.8}$	$10.4^{+2.8}_{-1.8}$	$5.3^{+1.7}_{-1.1}$
0 b jets Data	2919	1166	769	255	91	31	10	4
1 b jet SM	630^{+26}_{-25}	271^{+10}_{-16}	202^{+10}_{-6}	$78.0^{+6.9}_{-1.9}$	$24.2^{+2.9}_{-2.0}$	$10.6^{+1.7}_{-1.3}$	$2.9^{+0.9}_{-0.5}$	$2.2^{+0.7}_{-0.4}$
1 b jet Data	614	294	214	71	20	6	4	0
2 b jets SM	162^{+13}_{-12}	$61.8^{+4.8}_{-6.3}$	$58.8^{+4.8}_{-2.6}$	$28.0^{+3.5}_{-1.1}$	$9.0^{+1.4}_{-1.0}$	$7.1^{+1.4}_{-1.0}$	$0.6^{+0.3}_{-0.2}$	$0.9^{+0.4}_{-0.2}$
2 b jets Data	160	68	52	19	11	7	0	2
$\geq$ 3 b jets SM	$10.5^{+3.5}_{-2.2}$	$7.1^{+2.2}_{-1.8}$	$5.8^{+1.4}_{-0.9}$	$3.1^{+1.0}_{-0.7}$	$1.7^{+0.5}_{-0.4}$	$0.7^{+0.5}_{-0.4}$	$0.1^{+0.1}_{-0.1}$	$0.2^{+0.1}_{-0.1}$
$\geq$ 3 b jets Data	10	8	8	1	0	0	0	0

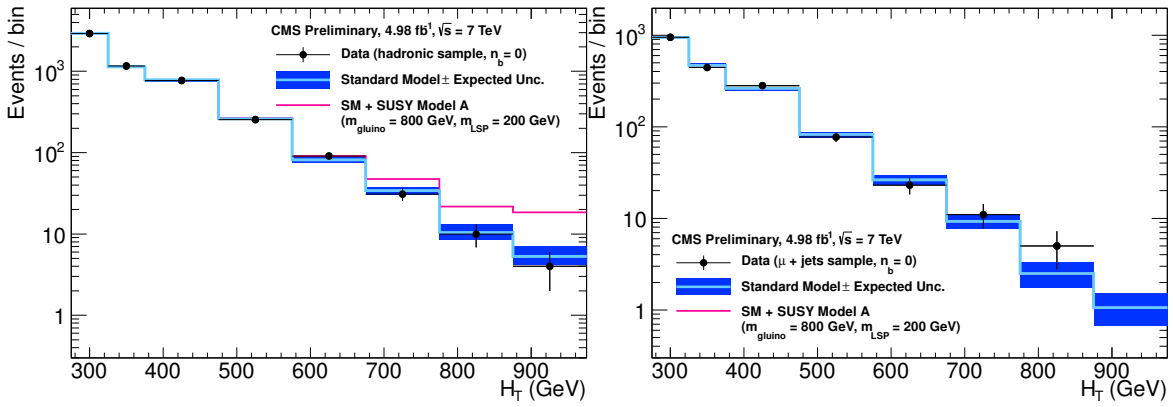

(a) Hadronic sample

(b) μ + jets sample

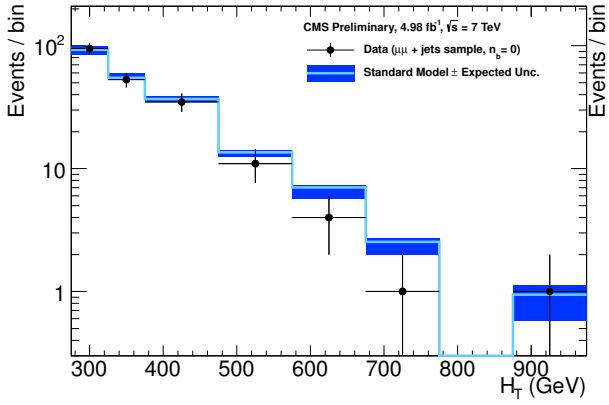

(c) $\mu\mu$ + jets sample

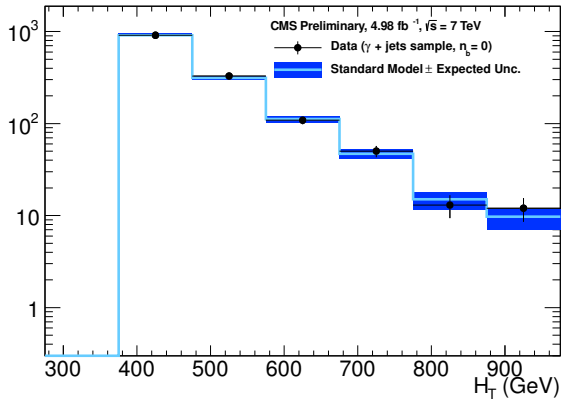

(d) γ + jets sample

Figure 2: Comparison of the observed yields and SM expectations given by the simultaneous fit in bins of H_T for the (a) hadronic, (b) μ + jets, (c) $\mu\mu$ + jets and (d) γ + jets samples when requiring exactly zero reconstructed b-jets. The observed event yields in data (black dots) and the expectations and their uncertainties, as determined by the simultaneous fit, for all SM processes (light blue solid line with dark blue bands) are shown. For illustrative purposes only, an example signal model is superimposed on the SM expectation (magenta solid line).

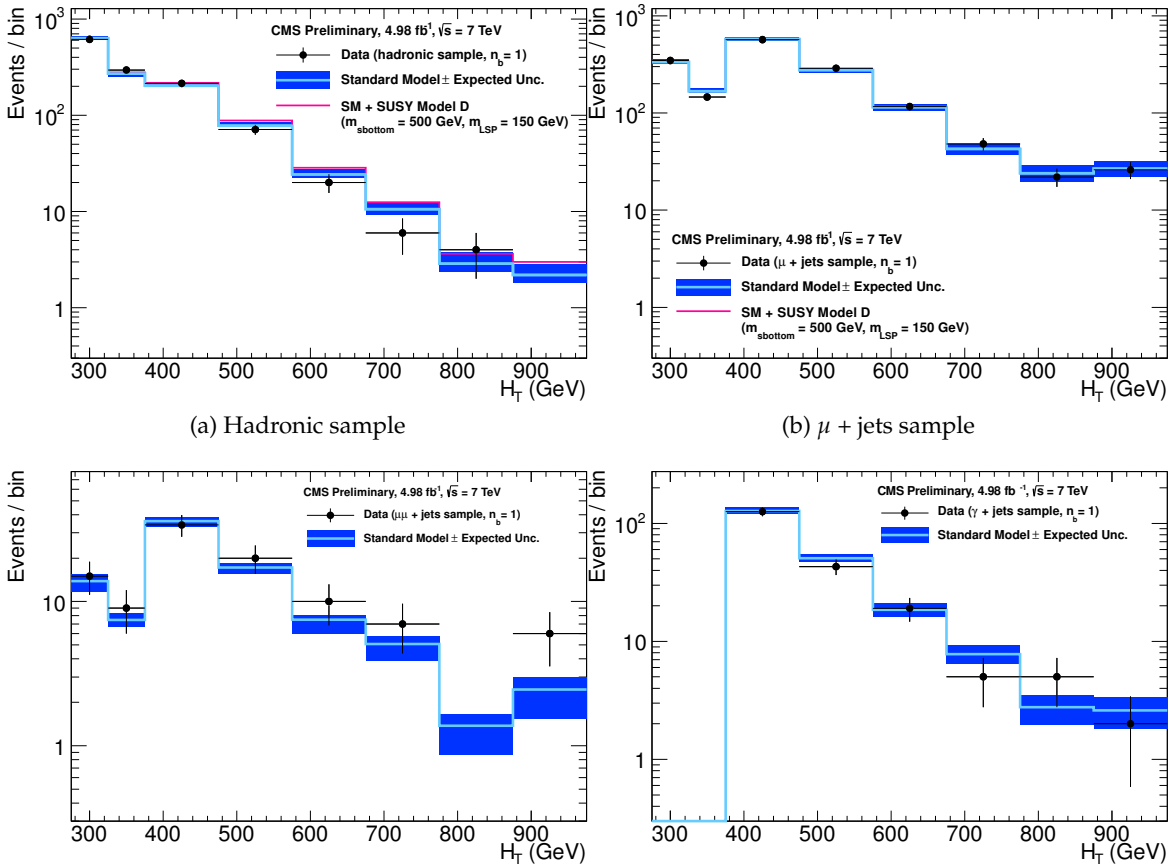

(a) Hadronic sample

(b) μ + jets sample

(c) $\mu\mu$ + jets sample

(d) γ + jets sample

Figure 3: Comparison of the observed yields and SM expectations given by the simultaneous fit in bins of H_T for the (a) hadronic, (b) μ + jets, (c) $\mu\mu$ + jets and (d) γ + jets samples when requiring exactly one reconstructed b-jet. The observed event yields in data (black dots) and the expectations and their uncertainties, as determined by the simultaneous fit, for all SM processes (light blue solid line with dark blue bands) are shown. For illustrative purposes only, an example signal model is superimposed on the SM expectation (magenta solid line).

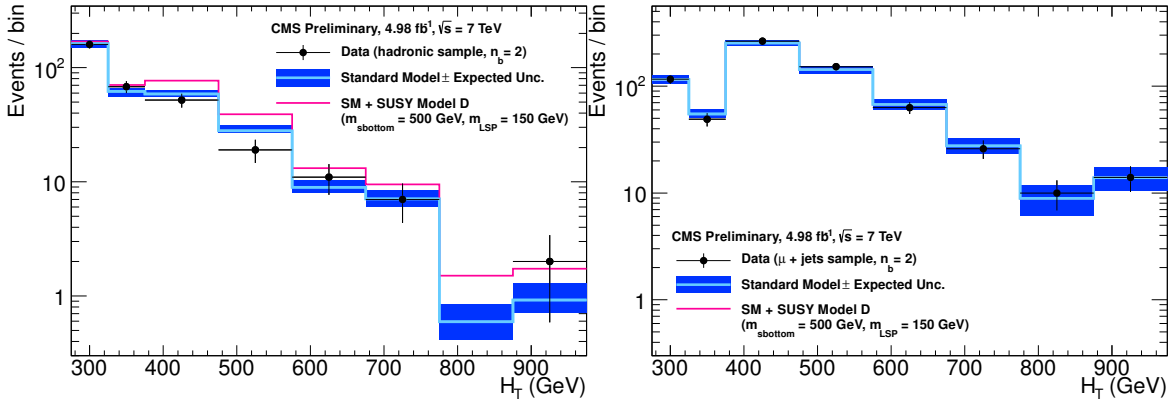

(a) Hadronic sample

(b) μ + jets sample

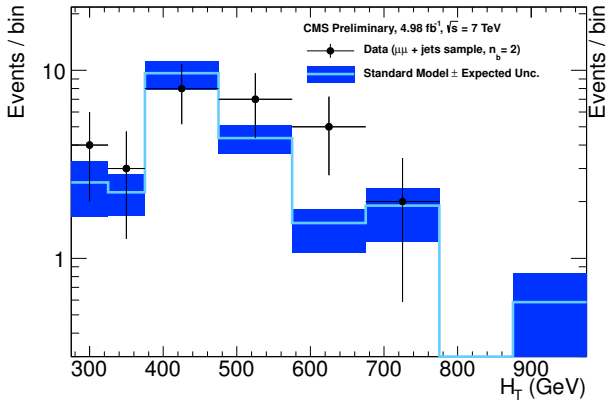

(c) $\mu\mu$ + jets sample

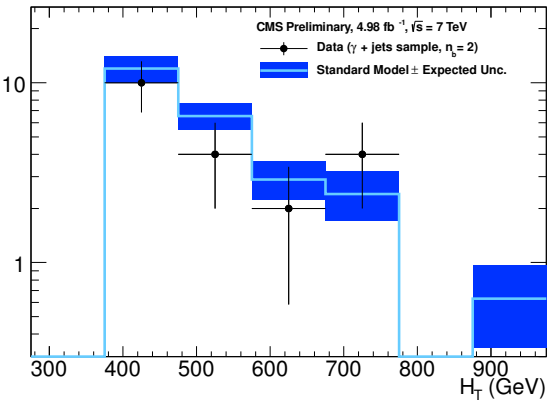

(d) γ + jets sample

Figure 4: Comparison of the observed yields and SM expectations given by the simultaneous fit in bins of H_T for the (a) hadronic, (b) μ + jets, (c) $\mu\mu$ + jets and (d) γ + jets samples when requiring exactly two reconstructed b-jets. The observed event yields in data (black dots) and the expectations and their uncertainties, as determined by the simultaneous fit, for all SM processes (light blue solid line with dark blue bands) are shown. For illustrative purposes only, an example signal model is superimposed on the SM expectation (magenta solid line).

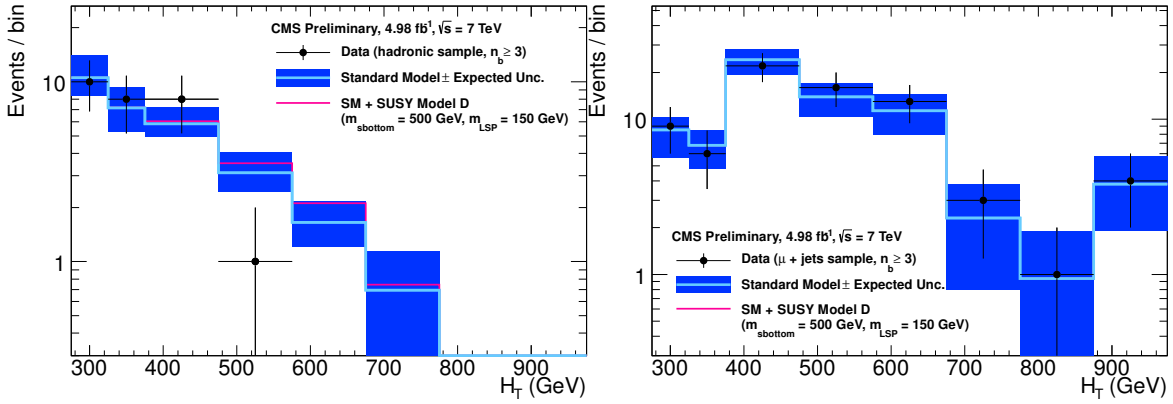

(a) Hadronic sample (b) μ + jets sample

Figure 5: Comparison of the observed yields and SM expectations given by the simultaneous fit in bins of H_T for the (a) hadronic and (b) μ + jets samples when requiring at least three reconstructed b-jets. The observed event yields in data (black dots) and the expectations and their uncertainties, as determined by the simultaneous fit, for all SM processes (light blue solid line with dark blue bands) are shown. For illustrative purposes only, an example signal model is superimposed on the SM expectation (magenta solid line).

7 Interpretation of the results

Limits are set in the parameter space of the CMSSM and in a set of simplified models that characterise both third-generation squark production and compressed SUSY spectra scenarios.

7.1 Interpretation in the CMSSM

At each point in the parameter space of the CMSSM, the SUSY particle spectrum is calculated with SOFTSUSY [45], and signal events are generated at leading order with PYTHIA 6.4 [42]. Inclusive, process-dependent, next-to-leading order calculations with next-to-leading logarithmic corrections [46] (NLO+NLL) of SUSY production cross sections are obtained with the program PROSPINO [47] and CTEQ6 [48] parton distribution functions. The simulated signal events are reweighted so that the distribution of the number of reconstructed vertices per beam crossing from the simulation matches that observed in data. Experimental uncertainties on the SM background prediction ($10-40\%$), the luminosity measurement (2.2%) [49], and the total acceptance times efficiency of the selection for the considered signal model (16%) are included in the calculation of the limit. The dominant sources of uncertainty on the signal efficiency times acceptance are derived from systematic variations of parton distribution functions, and corrections applied to jet energies and b jet efficiency and mistag rates. Although signal contributions to the total yield in each of the four considered data samples are allowed, the only relevant signal contribution originates from the hadronic data sample in the case of the CMSSM.

Figure 6 shows the observed and expected exclusion limits at 95% confidence level (CL) in the $(m_0, m_{1/2})$ plane for $\tan\beta = 10$ and $A_0 = 0$ GeV, calculated with NLO+NLL SUSY production cross sections and the CL_s method [50]. For this choice of parameter values, squark masses below 1250 GeV are excluded at 95% CL, as are gluino masses below the same value for the region $m_0 < 600$ GeV. In the region $600 < m_0 < 3000$ GeV, gluino masses below 700 GeV are excluded, while the limit on the squark mass varies in the range $1250-2500$ GeV, depending

on the value of m_0. The mass limits are determined with the observed limit for the nominal production cross section less 1σ theoretical uncertainty.

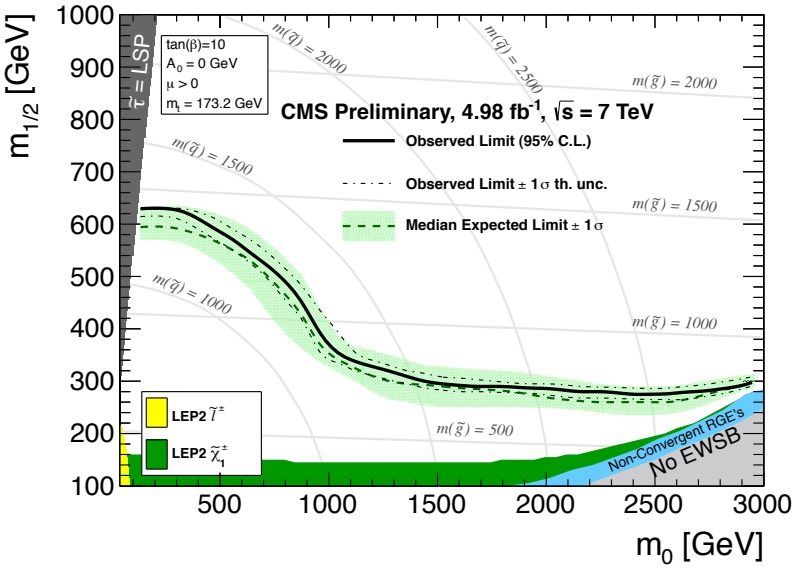

Figure 6: Exclusion contours at 95% CL in the CMSSM $(m_0, m_{1/2})$ plane ($\tan\beta = 10, A_0 = 0, \mu > 0$) calculated with NLO+NLL SUSY production cross sections and the CL_s method. The solid black line indicates the observed exclusion region. The dotted-dashed black lines represent the observed excluded region when varying the cross section by its theoretical uncertainty. The expected median exclusion region (green dashed line) $\pm 1\sigma$ (green band) are also shown. The CMSSM template is taken from Ref. [51].

7.2 Interpretation with simplified models

The data observations are also interpreted using simplified models that characterise third generation squark production and compressed SUSY spectra scenarios, where the mass difference between the primary produced sparticle (e.g. a squark or a gluino) and the LSP is rather small. The production and decay modes of the models under consideration are summarised in Table 2. The simplified models *A* and *B* are used to characterise the pair production of gluinos and first or second generation squarks, respectively, depending on their mass as well as on the LSP mass. Simplified models *C* to *F* describe various production and decay mechanisms in the context of third generation squarks.

Experimental uncertainties on the SM background predictions ($10-40\%$), the luminosity measurement (2.2%), and the total acceptance times efficiency of the selection for the considered signal model ($12\%-18\%$) are included in the calculation of the limit. Again, the presence of signal events in the control samples has been accounted for. Signal efficiency in the kinematic region defined by $0 < m_{\tilde{g}(\tilde{q})} - m_{\mathrm{LSP}} < 200\,\mathrm{GeV}$ or $m_{\tilde{g}(\tilde{q})} < 350\,\mathrm{GeV}$ is due in part to the presence of initial state radiation. Given the large associated uncertainties, no interpretation is provided for this kinematic region. In the case of model *E*, for which pair-produced gluinos decay to top-antitop quark pairs and the LSP, the region is enlarged to cover $0 < m_{\tilde{g}(\tilde{q})} - m_{\mathrm{LSP}} < 400\,\mathrm{GeV}$.

Table 2: The first three columns define the production and decay modes for various simplified models. The last two columns indicate the search sensitivity for these models, where $m^{\text{best}}_{\tilde{q}(\tilde{g})}$ and $m^{\text{best}}_{\text{LSP}}$ represent the largest mass beyond which no limit can be set for squarks/gluinos and the LSP, respectively. The exclusion range for $m_{\tilde{q}(\tilde{g})}$ is bounded from below by the kinematic region considered for each simplified model, as defined in the text. The only exception is model *C*, for which an exclusion can be set only for masses above ≈350 GeV. The quoted estimates are determined with the observed limit for the nominal production cross section less 1σ theoretical uncertainty.

Model	Production and decay modes	Figure	$m^{\text{best}}_{\tilde{q}(\tilde{g})}$ (GeV)	$m^{\text{best}}_{\text{LSP}}$ (GeV)
A	$pp \to \tilde{g}\tilde{g} \to q\bar{q}\tilde{\chi}^0 q\bar{q}\tilde{\chi}^0$	7a	≈950	≈400
B	$pp \to \tilde{q}\tilde{q} \to q\tilde{\chi}^0\bar{q}\tilde{\chi}^0$	7b	≈750	≈275
C	$pp \to \tilde{t}\bar{\tilde{t}} \to t\tilde{\chi}^0\bar{t}\tilde{\chi}^0$	7c	≈475	≈50
D	$pp \to \tilde{b}\bar{\tilde{b}} \to b\tilde{\chi}^0\bar{b}\tilde{\chi}^0$	7d	≈500	≈175
E	$pp \to \tilde{g}\tilde{g} \to t\bar{t}\tilde{\chi}^0 t\bar{t}\tilde{\chi}^0$	7e	≈850	≈250
F	$pp \to \tilde{g}\tilde{g} \to b\bar{b}\tilde{\chi}^0 b\bar{b}\tilde{\chi}^0$	7f	≈1025	≈550

Figure 7 shows the upper limit on the cross section at 95% CL as a function of $m_{\tilde{q}}$ or $m_{\tilde{g}}$ and m_{LSP} for various simplified models. The solid thick black line indicates the observed exclusion region assuming NLO+NLL [46, 47] SUSY cross section for squark pair production in the limit of decoupled gluinos (or vice versa). The thin black lines represent the observed excluded region when varying the cross section by its theoretical uncertainty. The dashed purple lines indicate the median (thick line) $\pm 1\sigma$ (thin lines) expected exclusion regions.

The most stringent mass limits on the pair-produced sparticles are obtained at low LSP masses, whilst the limits typically weaken for compressed spectra, i.e. points close to the diagonal. In particular, for all of the considered simplified models, there is an LSP mass beyond which no limit can be set. This is illustrated in Figure 7a, where the most stringent limit on the gluino mass is obtained at around 950 TeV for low LSP masses, whilst this limit weakens to below 900 GeV when the LSP mass reaches 350 GeV. For LSP masses above 400 GeV, no gluino masses can be excluded. Table 2 summarises these two extreme cases for models *A* to *F*. The estimates on the mass limits are determined with the observed limit for the nominal production cross section less 1σ theoretical uncertainty. No exclusion of direct top squark pair production (model *E*) assuming NLO+NLL production cross section is expected with the analysed dataset and for LSP masses greater than 50 GeV.

8 Summary

In summary, a search for supersymmetry based on a data sample of pp collisions collected at $\sqrt{s} = 7$ TeV, corresponding to an integrated luminosity of 4.98 fb^{-1}, has been reported. Final states with two or more jets and significant $\not{E}_{\text{T}}$, as expected from high-mass squark and gluino production and decays, have been analysed. An exclusive search has been performed in a binned signal region defined by the scalar sum of the transverse energy of jets, H_{T}, and the number of jets identified to originate from a bottom quark. The sum of standard model backgrounds per bin has been estimated from a simultaneous binned likelihood fit to hadronic, μ + jets, $\mu\mu$ + jets, and γ + jets samples. The observed yields are found to be in agreement with the expected contributions from standard model processes. Limits in the CMSSM $(m_0, m_{1/2})$ plane for $\tan\beta = 10$, $A_0 = 0$ GeV, and $\mu > 0$ have been derived. For this choice of parameter values, gluino masses below 700 GeV are excluded at 95% CL. The exclusion increases to 1250 GeV for squarks and gluinos of equal mass. Furthermore, exclusion limits are also set in simplified models, with a special emphasis on third generation and compressed spectra scenarios. In the

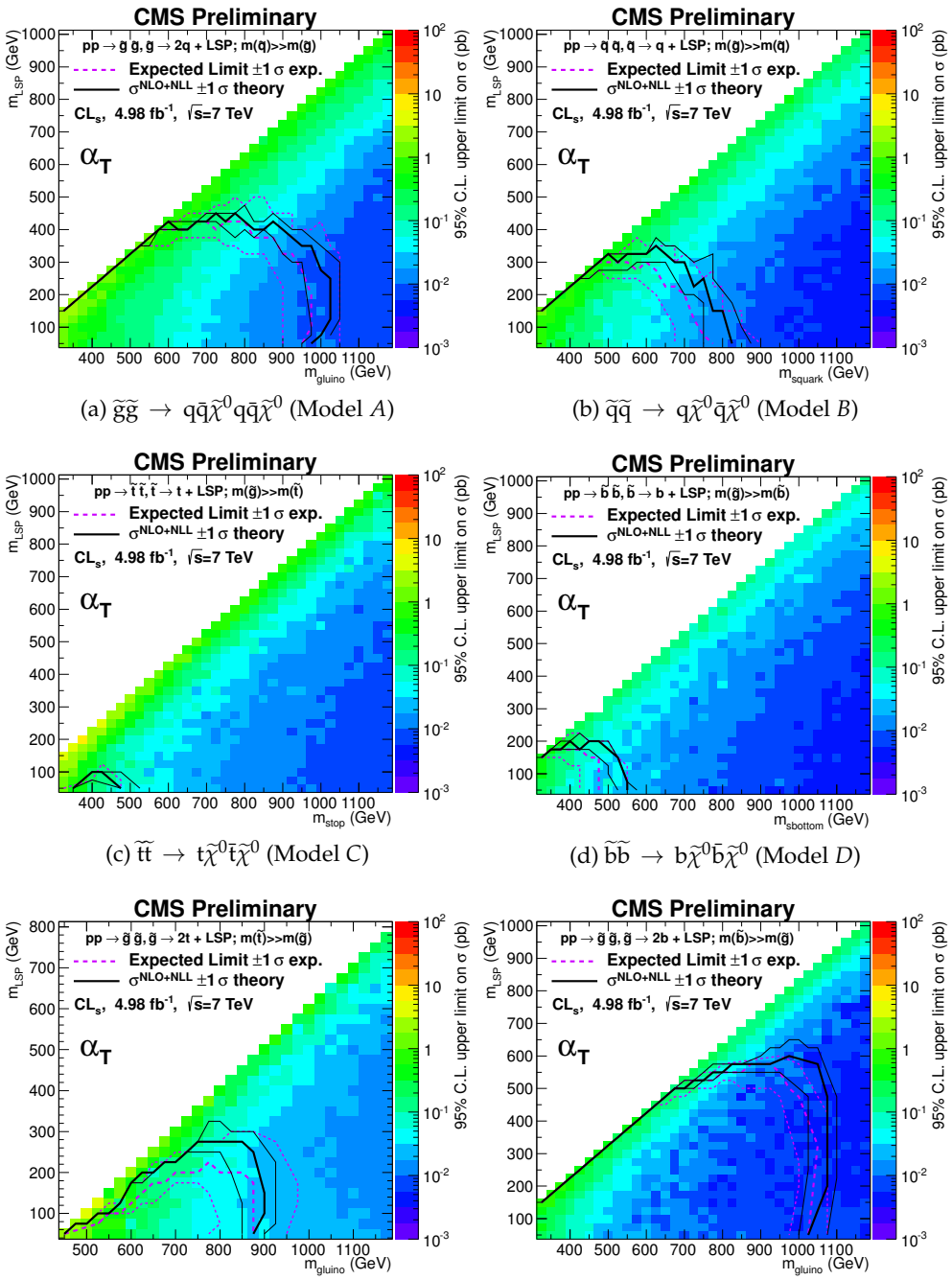

(a) $\tilde{g}\tilde{g} \rightarrow q\bar{q}\tilde{\chi}^0 q\bar{q}\tilde{\chi}^0$ (Model *A*)

(b) $\tilde{q}\tilde{q} \rightarrow q\tilde{\chi}^0\bar{q}\tilde{\chi}^0$ (Model *B*)

(c) $\tilde{t}\bar{\tilde{t}} \rightarrow t\tilde{\chi}^0\bar{t}\tilde{\chi}^0$ (Model *C*)

(d) $\tilde{b}\bar{\tilde{b}} \rightarrow b\tilde{\chi}^0\bar{b}\tilde{\chi}^0$ (Model *D*)

(e) $\tilde{g}\tilde{g} \rightarrow t\bar{t}\tilde{\chi}^0 t\bar{t}\tilde{\chi}^0$ (Model *E*)

(f) $\tilde{g}\tilde{g} \rightarrow b\bar{b}\tilde{\chi}^0 b\bar{b}\tilde{\chi}^0$ (Model *F*)

Figure 7: Upper limit on cross section at 95% CL as a function of $m_{\tilde{q}}$ or $m_{\tilde{g}}$ and m_{LSP} for various simplified models. The solid thick black line indicates the observed exclusion region assuming NLO+NLL SUSY production cross section. The thin black lines represent the observed excluded region when varying the cross section by its theoretical uncertainty. The dashed purple lines indicate the median (thick line) $\pm 1\sigma$ (thin lines) expected exclusion regions.

considered models with gluino pair production and for small LSP masses, typical exclusion limits of the gluino mass are around 1 TeV. For simplified models with squark pair production, first or second generation squarks are excluded up to around 750 GeV and bottom squarks are excluded up to around 500 GeV, again for small LSP masses. However, for the simplified models under consideration, the most constraining limit on the LSP mass is significantly below 1 TeV, indicating that a large range of SUSY parameter space is yet to be probed by the LHC.

9 Acknowledgements

We congratulate our colleagues in the CERN accelerator departments for the excellent performance of the LHC machine during 2011. We thank the technical and administrative staff at CERN and other CMS institutes, and acknowledge support from: FMSR (Austria); FNRS and FWO (Belgium); CNPq, CAPES, FAPERJ, and FAPESP (Brazil); MES (Bulgaria); CERN; CAS, MoST, and NSFC (China); COLCIENCIAS (Colombia); MSES (Croatia); RPF (Cyprus); Academy of Sciences and NICPB (Estonia); Academy of Finland, ME, and HIP (Finland); CEA and CNRS/IN2P3 (France); BMBF, DFG, and HGF (Germany); GSRT (Greece); OTKA and NKTH (Hungary); DAE and DST (India); IPM (Iran); SFI (Ireland); INFN (Italy); NRF and WCU (Korea); LAS (Lithuania); CINVESTAV, CONACYT, SEP, and UASLP-FAI (Mexico); PAEC (Pakistan); SCSR (Poland); FCT (Portugal); JINR (Armenia, Belarus, Georgia, Ukraine, Uzbekistan); MST and MAE (Russia); MSTD (Serbia); MICINN and CPAN (Spain); Swiss Funding Agencies (Switzerland); NSC (Taipei); TUBITAK and TAEK (Turkey); STFC (United Kingdom); DOE and NSF (USA).

References

[1] Y. A. Gol'fand and E. P. Likhtman, "Extension of the Algebra of Poincaré Group Generators and Violation of p Invariance", *JETP Lett.* **13** (1971) 323.

[2] J. Wess and B. Zumino, "Supergauge transformations in four dimensions", *Nucl. Phys. B* **70** (1974) 39, doi:10.1016/0550-3213(74)90355-1.

[3] H. P. Nilles, "Supersymmetry, Supergravity and Particle Physics", *Phys. Reports* **110** (1984) 1, doi:10.1016/0370-1573(84)90008-5.

[4] H. Haber and G. Kane, "The Search for Supersymmetry: Probing Physics Beyond the Standard Model", *Phys. Reports* **117** (1987) 75, doi:10.1016/0370-1573(85)90051-1.

[5] R. Barbieri, S. Ferrara, and C. A. Savoy, "Gauge Models with Spontaneously Broken Local Supersymmetry", *Phys. Lett. B* **119** (1982) 343, doi:10.1016/0370-2693(82)90685-2.

[6] S. Dawson, E. Eichten, and C. Quigg, "Search for Supersymmetric Particles in Hadron - Hadron Collisions", *Phys. Rev. D* **31** (1985) 1581, doi:10.1103/PhysRevD.31.1581.

[7] E. Witten, "Dynamical Breaking of Supersymmetry", *Nucl. Phys. B* **188** (1981) 513, doi:10.1016/0550-3213(81)90006-7.

[8] S. Dimopoulos and H. Georgi, "Softly Broken Supersymmetry and SU(5)", *Nucl. Phys. B* **193** (1981) 150, doi:10.1016/0550-3213(81)90522-8.

[9] R. Barbieri and D. Pappadopulo, "S-particles at their naturalness limits", *JHEP* **10** (2009) doi:10.1088/1126-6708/2009/10/061, arXiv:0906.4546.

[10] G. R. Farrar and P. Fayet, "Phenomenology of the Production, Decay, and Detection of New Hadronic States Associated with Supersymmetry", *Phys. Lett. B* **76** (1978) 575, doi:10.1016/0370-2693(78)90858-4.

[11] CMS Collaboration Collaboration, "Search for Supersymmetry at the LHC in Events with Jets and Missing Transverse Energy", *Phys. Rev. Lett.* **107** (Nov, 2011) 221804, doi:10.1103/PhysRevLett.107.221804.

[12] CMS Collaboration, "Search for Supersymmetry in pp Collisions at 7 TeV in Events with Jets and Missing Transverse Energy", *Phys. Lett.* **B698** (2011) 196–218, doi:10.1016/j.physletb.2011.03.021, arXiv:1101.1628.

[13] CMS Collaboration, "Search for new physics with jets and missing transverse momentum in pp collisions at $\sqrt{s} = 7$ TeV", *JHEP* **2011** (2011) 1–46. 10.1007/JHEP08(2011)155.

[14] CMS Collaboration, "Inclusive search for squarks and gluinos in pp collisions at $\sqrt{s} = 7$ TeV", *Phys. Rev. D* **85** (Jan, 2012) 012004, doi:10.1103/PhysRevD.85.012004.

[15] CMS Collaboration, "Search for supersymmetry in events with b jets and missing transverse momentum at the LHC", *JHEP* **2011** (2011) 1–26. 10.1007/JHEP07(2011)113.

[16] ATLAS Collaboration, "Search for squarks and gluinos using final states with jets and missing transverse momentum with the ATLAS detector in proton-proton collisions", *Physics Letters B* **710** (2012), no. 1, 67 – 85, doi:10.1016/j.physletb.2012.02.051.

[17] ATLAS Collaboration, "Search for new phenomena in final states with large jet multiplicities and missing transverse momentum using $\sqrt{s}$ = 7 TeV pp collisions with the ATLAS detector", *JHEP* **2011** (2011) 1–38. 10.1007/JHEP11(2011)099.

[18] ATLAS Collaboration, "Search for Scalar Bottom Quark Pair Production with the ATLAS Detector in pp Collisions at $\sqrt{s}$ = 7 TeV", *Phys. Rev. Lett.* **108** (May, 2012) 181802, doi:10.1103/PhysRevLett.108.181802.

[19] ATLAS Collaboration, "Search for squarks and gluinos using final states with jets and missing transverse momentum with the ATLAS detector in proton-proton collisions", *Physics Letters B* **701** (2011), no. 2, 186 – 203, doi:10.1016/j.physletb.2011.05.061.

[20] A. H. Chamseddine, R. Arnowitt, and P. Nath, "Locally Supersymmetric Grand Unification", *Phys. Rev. Lett.* **49** (1982) 970, doi:10.1103/PhysRevLett.49.970.

[21] R. Arnowitt and P. Nath, "Supersymmetric mass spectrum in SU(5) supergravity grand unification", *Phys. Rev. Lett.* **69** (1992) 725, doi:10.1103/PhysRevLett.69.725.

[22] G. L. Kane et al., "Study of constrained minimal supersymmetry", *Phys. Rev. D* **49** (1994) 6173, doi:10.1103/PhysRevD.49.6173.

[23] J. Alwall, P. Schuster, and N. Toro, "Simplified Models for a First Characterization of New Physics at the LHC", *Phys. Rev.* **D79** (2009) 075020, doi:10.1103/PhysRevD.79.075020, arXiv:0810.3921.

[24] J. Alwall, M.-P. Le, M. Lisanti et al., "Model-Independent Jets plus Missing Energy Searches", *Phys.Rev.* **D79** (2009) 015005, doi:10.1103/PhysRevD.79.015005, arXiv:0809.3264.

[25] D. Alves, N. Arkani-Hamed, S. Arora et al., "Simplified Models for LHC New Physics Searches", arXiv:1105.2838. Official summary of results from the 'Topologies for Early LHC Searches' workshop, SLAC, September 2010.

[26] CMS Collaboration, "The CMS experiment at the CERN LHC", *JINST* **03** (2008) S08004, doi:10.1088/1748-0221/3/08/S08004.

[27] M. Cacciari, G. P. Salam, and G. Soyez, "The anti-k_T jet clustering algorithm", *JHEP* **04** (2008) 063, doi:10.1088/1126-6708/2008/04/063.

[28] CMS Collaboration Collaboration, "Determination of Jet Energy Calibration and Transverse Momentum Resolution in CMS", *JINST* **6** (2011) P11002, doi:10.1088/1748-0221/6/11/P11002, arXiv:1107.4277.

[29] CMS Collaboration, "Identification and filtering of uncharacteristic noise in the CMS hadron calorimeter", *JINST* **5** (2010) T03014, doi:10.1088/1748-0221/5/03/T03014.

[30] CMS Collaboration, "Electromagnetic calorimeter commissioning and first results with 7 TeV data", CMS Note CMS-NOTE-2010-012, CMS, (2010).

[31] CMS Collaboration, "Electron reconstruction and identification at $\sqrt{s} = 7$ TeV", CMS Physics Analysis Summary EGM-10-004, CMS, (2010).

[32] CMS Collaboration, "Performance of muon identification in pp collisions at $\sqrt{s} = 7$ TeV", CMS Physics Analysis Summary MUO-10-002, CMS, (2010).

[33] CMS Collaboration, "Isolated Photon Reconstruction and Identification at $\sqrt{s} = 7$ TeV", CMS Physics Analysis Summary EGM-10-006, CMS, (2010).

[34] CMS Collaboration, "b-Jet Identification in the CMS Experiment", CMS Physics Analysis Summary BTV-11-004, CMS, (2012).

[35] CMS Collaboration, "Measurement of btagging efficiency using ttbar events", CMS Physics Analysis Summary BTV-11-003, CMS, (2012).

[36] L. Randall and D. Tucker-Smith, "Dijet Searches for Supersymmetry at the Large Hadron Collider", *Phys. Rev. Lett.* **101** (2008) 221803, doi:10.1103/PhysRevLett.101.221803.

[37] CMS Collaboration, "SUSY searches with dijet events", CMS Physics Analysis Summary SUS-08-005, CMS, (2008).

[38] CMS Collaboration, "Search strategy for exclusive multi-jet events from supersymmetry at CMS", CMS Physics Analysis Summary SUS-09-001, CMS, (2009).

[39] CMS Collaboration, "Data-Driven Estimation of the Invisible Z Background to the SUSY MET Plus Jets Search", CMS Physics Analysis Summary SUS-08-002, CMS, (2008).

[40] Z. Bern, G. Diana, L. Dixon et al., "Driving Missing Data at Next-to-Leading Order", *Phys.Rev.* **D84** (2011) 114002, doi:10.1103/PhysRevD.84.114002, arXiv:1106.1423.

[41] CMS Collaboration, "First Measurement of the Cross Section for Top-Quark Pair Production in Proton-Proton Collisions at $\sqrt{s}$ = 7 TeV", *Phys. Lett. B* **695** (2011) 424, doi:10.1016/j.physletb.2010.11.058.

[42] T. Sjöstrand, S. Mrenna and P. Z. Skands, "PYTHIA 6.4 Physics and Manual", *JHEP* **05** (2006) 026, doi:10.1088/1126-6708/2006/05/026.

[43] J. Alwall et al., "MadGraph/MadEvent v4: The New Web Generation", *JHEP* **09** (2007) 028, arXiv:0706.2334.

[44] GEANT4 Collaboration, "GEANT4: A simulation toolkit", *Nucl. Instrum. Meth.* **A506** (2003) 250–303, doi:10.1016/S0168-9002(03)01368-8.

[45] B. C. Allanach, "SOFTSUSY: a program for calculating supersymmetric spectra", *Comput. Phys. Commun.* **143** (2002) 305, doi:10.1016/S0010-4655(01)00460-X.

[46] M. Krämer, A. Kulesza, R. van der Leeuw et al., "Supersymmetry production cross sections in pp collisions at $\sqrt{s} = 7$ TeV", arXiv:1206.2892.

[47] W. Beenakker et al., "Squark and gluino production at hadron colliders", *Nucl. Phys. B* **492** (1997) 51, doi:10.1016/S0550-3213(97)00084-9.

[48] J. Pumplin et al., "New generation of parton distributions with uncertainties from global QCD analysis", *JHEP* **07** (2002) 012, arXiv:hep-ph/0201195.

[49] CMS Collaboration, "Measurement of CMS Luminosity", CMS Physics Analysis Summary EWK-10-004, CMS, (2010).

[50] Particle Data Group Collaboration, "Review of particle physics", *J. Phys. G* **37** (2010) 075021, doi:10.1088/0954-3899/37/7A/075021.

[51] K. Matchev and R. Remington, "Updated templates for the interpretation of LHC results on supersymmetry in the context of mSUGRA", arXiv:1202.6580.